Climate Dynamics (2023) 61:2921–2936
https://doi.org/10.1007/s00382-023-06704-y

Future changes of circulation types and their effects on surface air temperature and precipitation in the SMHI large ensemble

Felicitas Hansen[1,2] · Danijel Belušić[2,3] · Klaus Wyser[2] · Torben Koenigk[2]

Received: 8 June 2022 / Accepted: 4 February 2023 / Published online: 2 March 2023

Abstract
Being strongly influenced by internal climate variability, the atmospheric circulation response to greenhouse gas forcing in the future climate is uncertain. This study addresses atmospheric circulation through representative circulation types (CTs) and investigates the CTs' changes with respect to frequency and effect on surface temperature and precipitation over a pan-Scandinavian domain. The analysis is based on the Swedish Meteorological and Hydrological Institute Large Ensemble performed with EC-Earth3: 50-member ensembles from one historical and six scenario simulations for the twenty-first century are used to assess internal variability and significance of changes. Although the results show no strong future changes in the CTs' sea level pressure patterns, CT frequency changes suggest a future extension of summer conditions towards spring and autumn and point towards a clearer distinction between summer and winter. The present-climate CT effect on surface temperature is found to generally weaken which is consistent with a general decrease in temperature variability. Largest-scale and strongest temperature effect changes are projected between March and May for CT3, a cyclone towards the east of the domain associated with a domain-wide cooling effect that will likely be decreased towards the end of the twenty-first century. Similarly but of opposite sign, the CT effect on precipitation is strengthening as a result of the increased precipitation variability. Here, largest-scale and strongest effect enhancement is found for CT6, thus increasing its wetting effect over southern Scandinavia and drying effect west of the Scandes. Changes are generally largest towards the end of the twenty-first century and tend to increase with the forcing strength, thus maximizing for SSP585.

Keywords Circulation type changes · Climate change · Large ensemble · Scandinavia · Circulation type classification · EC-Earth

1 Introduction

The large-scale atmospheric circulation is one of the most important factors influencing weather and climate conditions on various timescales. Its short- and long-term variations are directly linked to both the mean and extreme values of surface parameters like temperature and precipitation rates. With the global climate changing due to anthropogenic greenhouse gases (IPCC 2021) it is hence of particular interest to investigate potential changes of atmospheric circulation patterns, also because these may significantly alter or amplify the expected thermodynamic changes.

The atmospheric circulation can, e.g., be described by sea level pressure (SLP) fields, and every such field represents one individual and unique example for its complex appearance. To investigate changes in the atmospheric circulation it is, however, useful to condense the circulation's main aspects into a reasonably small set of representative dynamical situations. Circulation type classification (CTC) methods are often used in this context where circulation patterns that show defined similarities are combined into one class, with the class represented by the average of all its members, i.e., the circulation type (CT). A wide range of CTC methods exists [see, e.g., Philipp et al. (2010) for a comprehensive description and comparison] and can be roughly divided into two groups: those that assign individual circulation patterns to some kind of predefined CTs, and those where the CTs are

✉ Felicitas Hansen
felicitas.hansen@hereon.de

[1] Institute of Coastal Systems, Helmholtz-Zentrum Hereon, Geesthacht, Germany

[2] Rossby Centre, Swedish Meteorological and Hydrological Institute, Norrköping, Sweden

[3] Department of Geophysics, Faculty of Science, University of Zagreb, Zagreb, Croatia

derived as part of an automated process. Both groups have their advantages depending on specific applications, but generally there is no particular CTC method which could be considered "the truth" (Huth et al. 2007). However, the simulated annealing and diversified randomization (SANDRA) classification scheme (Philipp et al. 2007) has been shown to overcome many of the limitations of other CTC methods while at the same time being less numerically expensive. In SANDRA, similarities between individual circulation patterns are measured by the Euclidean distance between fields. Hansen and Belušić (2021) have recently shown that applying a Euclidean distance-based classification method like SANDRA to input data where the spatial mean is removed from each field leads to high physical consistency between members of one class and effective performance in partitioning dependent surface parameters like temperature or precipitation. We follow these findings and use SANDRA with daily SLP spatial anomaly fields to analyse future changes of CTs over a pan-Scandinavian domain.

Two aspects of future CT changes are of particular interest. The first one involves changes in frequency of the individual CTs; having, e.g., more or less westerly circulation situations or more or less blockings over a specific domain can have strong implications for regional and local weather and climate conditions. This includes consequences for extremes like cold winters (Cattiaux et al. 2010) or warm summers (Wilcke et al. 2020). The second aspect includes changes in the link between circulation and local climate, or the "effect" that the individual CTs have on dependent variables like surface temperature or precipitation rates. A stable or stationary relation between the large-scale circulation and the local climate is required to assess future regional climate changes through statistical downscaling of the large-scale patterns. Hence, if the local effects of a CT changed with time, such an assessment would not be justified.

Projections of the future climate are associated with uncertainties stemming from three major sources. Uncertainties in the next decade are dominated by internal atmospheric variability (Hawkins and Sutton 2009; Koenigk et al. 2020), which itself in the middle and high latitudes can have its sources in the variability of the annular modes (Deser et al. 2012; Horton et al. 2015), the El Nino Southern Oscillation (Trenberth et al. 1997; Ineson and Scaife 2009), North Atlantic sea surface temperature variability (e.g. Schlesinger and Ramankutty 1994), the Pacific Decadal Oscillation (Mantua et al. 1997), Arctic sea ice variations (Dai and Blöcker 2019) or variability in the stratosphere (Baldwin et al. 2001; Waugh et al. 2017). Towards the end of the twenty-first century the uncertainty in future climate trends is dominated by external forcings like emissions of climate-relevant greenhouse gases and other socio-economic developments. In future climate projections, these uncertainties are addressed by performing and analysing climate model simulations under different forcing scenarios such as the Shared Socioecomic Pathways (SSPs) or the preceding Representative Concentration Pathways (van Vuuren et al. 2011) or Special Report on Emission Scenarios (Nakicenovic et al. 2000). A third source of uncertainty associated with future climate projections, most pronounced around the middle of the twenty-first century, comes from errors in the models. These are often accounted for by analysing multi-model ensembles such as those provided in the Coupled Model Intercomparison Project (CMIP) framework.

In the present analyses of CT future climate changes, we are using the unique single-model large ensemble of future climate projections created at the Swedish Meteorological and Hydrological Institute (SMHI-LENS; Wyser et al. 2021), accounting for two out of three above-mentioned uncertainty sources: the external forcing uncertainties are addressed by providing eight different scenario simulations forced with different SSPs for the twenty-first century, while the uncertainties related to internal variability are accounted for by providing 50 realizations for each of the scenarios which were started from slightly different boundary conditions. There are other large ensembles available, performed in the CMIP5 and CMIP6 context and listed in the Multi Model Large Ensemble Archive (https://www.cesm.ucar.edu/projects/community-projects/MMLEA/, Deser et al. 2020). To our knowledge, the SMHI-LENS is currently the only large ensemble with a large number of ensemble members for all eight Tier 1 and Tier 2 ScenarioMIP emission scenarios (O'Neill et al. 2016) allowing for the analysis of a broad range of mitigation actions including the mitigation according to the Paris agreement, delayed mitigation and no mitigation.

The broad range of potential future pathways is particularly interesting for the investigation of circulation type changes as those have so far been mainly analyzed with respect to past changes (e.g. Beck et al. 2007; Cahynova and Huth 2016; Fernandez-Montes et al. 2012; Fleig et al. 2015; Jones and Lister 2009; Kucerova et al. 2017; Kuettel et al. 2011; Murawski et al. 2016; Stryhal and Huth 2019a, b; Kjellström et al. 2022), or using CMIP simulations under one (Stryhal and Huth 2019b; Huguenin et al. 2020) or a maximum of three RCP scenarios (Jacobeit et al. 2009). While many of these studies focus on one or two seasons, especially the winter season where the connection between the large-scale circulation and the surface weather and climate is strongest (Beck and Philipp 2010), we compute CTs from year-round SMHI-LENS SLP fields and attempt to identify future changes that are specific to the individual seasons. For example, summers might experience predominantly those CTs that occur less often in the other seasons and can hence be called "summer-CTs". If the frequency of these "summer-CTs" increases in spring and/or autumn in the twenty-first century, this could be interpreted as an

extension of summer (as defined in the present climate), thus a climatic change of the seasons.

This paper is exploiting the coexistence of three types of variability in the SMHI-LENS, i.e. variabilities stemming from (1) the different future scenarios, (2) the 50 ensemble members in each scenario and (3) the annual cycle. We investigate changes in the frequency and the effect of CTs on surface temperature and precipitation between future and present climate over a pan-Scandinavian domain, accounting for their uncertainties. Two future periods are considered independently, the middle and the end of the twenty-first century. Changes in the average effect of specific circulation types on the local weather and climate can have implications for changes in extremes, e.g. heatwaves, storms or extreme precipitation events, and are hence of interest not only from a scientific, but also from a societal and economic perspective.

2 Data and Methods

2.1 SMHI-large ensemble

The design of the SMHI Large Ensemble (SMHI-LENS) is described in Wyser et al. (2021). The ensemble consists of 50 members for each of the experiments described below, done with the coupled global climate model EC-Earth3 that was used for CMIP6. The atmosphere model used in EC-Earth3 is the Integrated Forecast System (IFS) cycle36r4, and for the ocean and sea ice components, the Nucleus for European Modelling of the Ocean (NEMO, version 3.6), including the sea ice model LIM3, has been used. The resolution of the coupled atmosphere–ocean model is approximately 0.8 degrees in the atmosphere and 1 degree in the ocean with refinement at the equator. Vertically, there are 91 levels in the atmosphere with the top level at 0.01 hPa, and 75 layers in the ocean with an upper level of about 1 m and 24 levels distributed over the uppermost 100 m. A detailed description of the EC-Earth3 model is provided in Döscher et al. (2022). Different from the CMIP6 protocol, the historical experiment of SMHI-LENS started from a set of 50 different initial conditions in 1970. This set of initial conditions was created from a set of six historical experiments that was done previously for CMIP6 and captures the full spread of the model's internal variability. The generation of the initial conditions for SMHI-LENS is described in detail in Wyser et al. (2021). The scenario experiments branched off in 2015, seamlessly continuing the historical simulation. While only 4 different scenarios were mentioned in Wyser et al. (2021) the SMHI-LENS has been expanded since and now includes all Tier 1 and Tier 2 ScenarioMIP scenarios (O'Neill et al. 2016). For the transient greenhouse gas, aerosol, and land use forcing the SMHI-LENS uses the datasets provided for ScenarioMIP.

Of the eight available SMHI-LENS scenarios, we use the following six in this study: SSP5-8.5, yielding the strongest global warming trend of all analyzed scenarios, SSP1-1.9, representing the lower end of a potential climate evolution, SSP5-3.4-OS, an overshoot scenario which follows the SSP5-8.5 scenario until 2040 and includes a decrease in emissions thereafter, and three scenarios that have a warming trend between the strong SSP5-8.5 and the weak SSP1-1.9 scenario (SSP3-7.0, SSP2-4.5 and SSP4-3.4). For convenience, we leave out the punctuation in the scenario names in the following, i.e. SSP585, SSP534OS and so on. For each of the scenarios, we compute classification types for a pan-Scandinavian domain (50°–73° N, 0°–30° E; see Sect. 2.2). The evolution of surface temperature (TAS) and precipitation (PR) averaged over this domain can be seen from Fig. 1 for all scenarios.

2.2 Circulation type classification

We are using the Simulated Annealing and Diversified Randomization (SANDRA; Philipp et al. 2010) method implemented in the COST733 software package to compute 10 SLP CTs over the pan-Scandinavian domain (the domain extent is seen in Figs. 2 and 3). SANDRA belongs to the CTC group of automated or optimization methods (Philipp et al. 2020) and is based on conventional k-means clustering. It extends k-means clustering by implementing two additional concepts: (1) the diversified randomization concept which randomizes the starting CTs as well as the ordering of input SLP fields and CT numbers throughout the iterative process of checking and reassigning, and (2) the concept of simulated annealing which allows input SLP fields to be temporarily assigned to specific CTs even though this results in a temporary decrease of the overall data partitioning quality (Philipp et al. 2007). With these additions, SANDRA has been shown to obtain results which are closer to the "global optimum" compared to e.g. k-means clustering and to overcome many of the limitations of established CTC methods while at the same time being less numerically expensive. As a result, SANDRA has become a widely used alternative to previously established CTC methods being applied to SLP or geopotential height fields in various contexts of atmospheric circulation studies (e.g. Jacobeit et al. 2017; Kuettel et al. 2011; Murawski et al. 2016; Meredith et al. 2018; Røste and Landgren 2022).

The SMHI-LENS data analysed for this study include 20 years (1995–2014) of a historical simulation and six scenarios for two future 20-years periods (2041–2060 and 2081–2100), each with daily year-round data of 50 ensemble members. Classifying these more than 4.7 million SLP fields together is computationally very challenging.

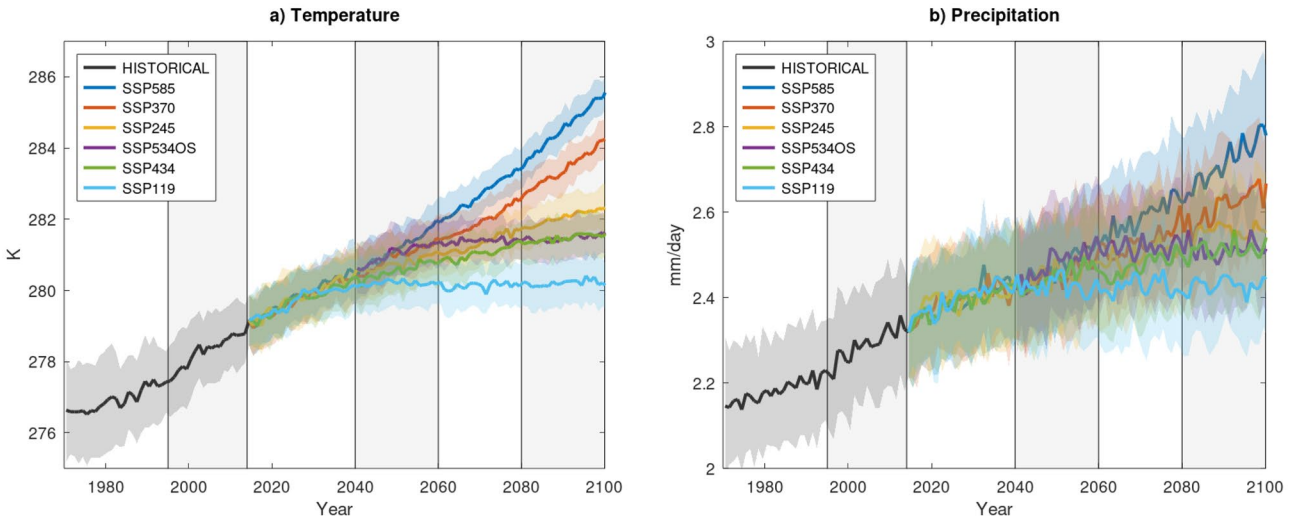

Fig. 1 Time series of annual mean **a** temperatures and **b** precipitation averaged over the pan-Scandinavian domain considered in this study (50°–73° N, 0°–30° E) for the historical and the six SSP scenario simulations. The thick lines are the ensemble averages over all respective 50 ensemble members, the shadings denote the +/−1 standard deviation range around the ensemble mean

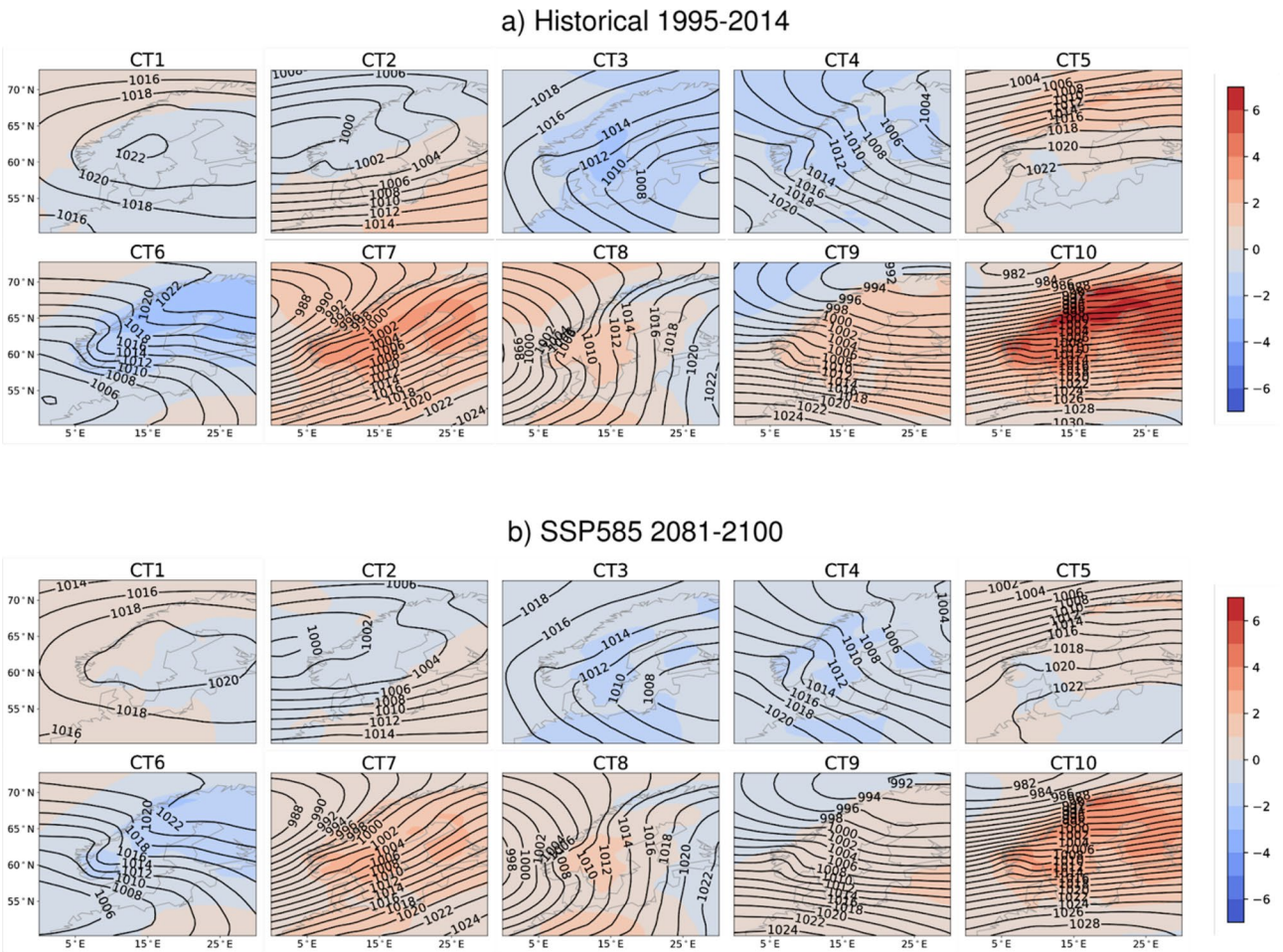

Fig. 2 SLP fields (contours; in hPa) and TAS anomalies (color; in K) for 10 CTs generated using 20 years of daily year-round SLP fields from 50 ensemble members of **a** the historical simulation between 1995 and 2014 and **b** the SSP585 scenario between 2081 and 2100. TAS anomalies are computed with respect to the climatological annual cycle over the 20 years for each ensemble member separately

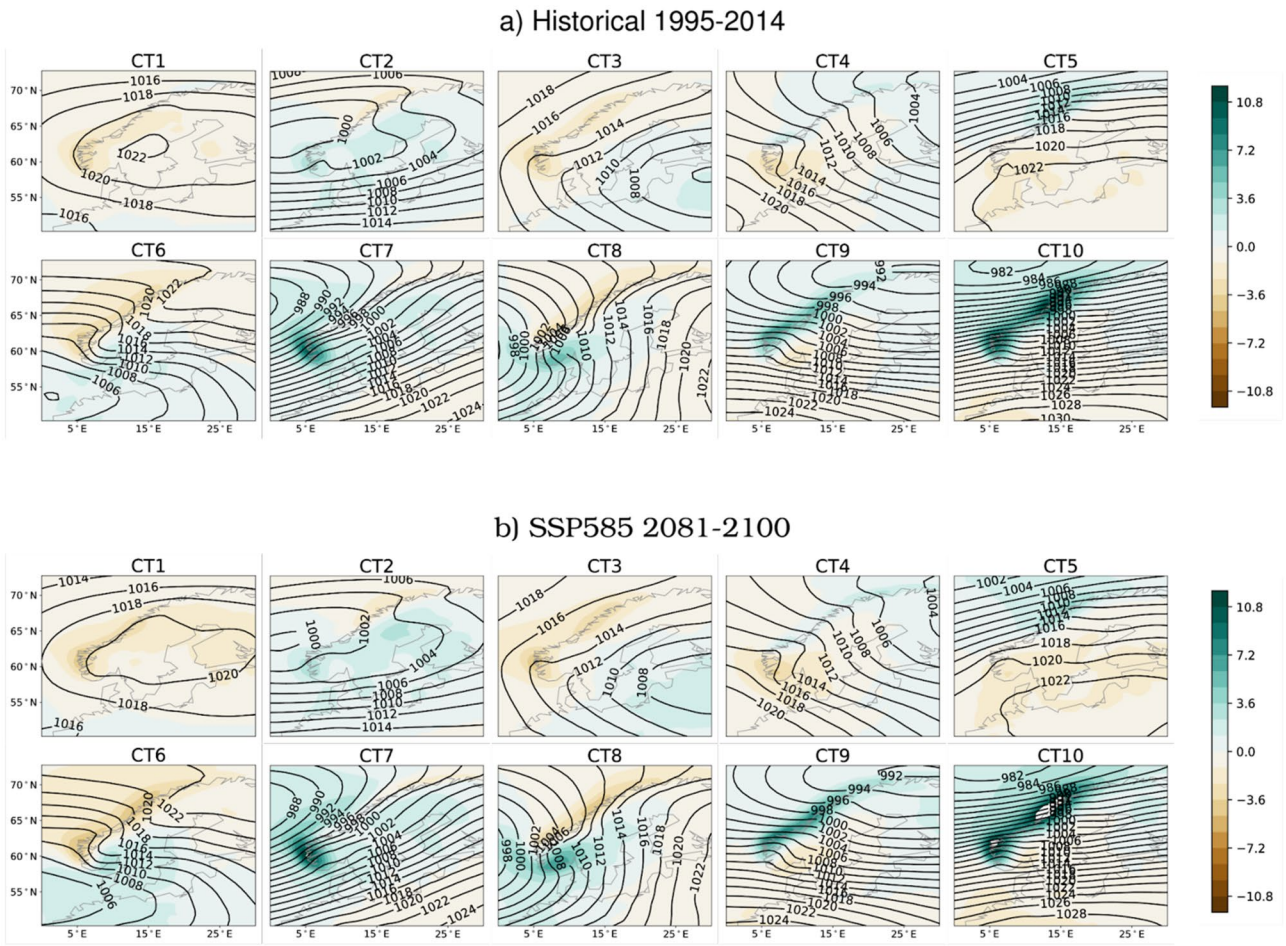

Fig. 3 Same as Fig. 2 but for PR anomalies (in mm/day)

Therefore, instead of performing the full classification on the entire SMHI-LENS dataset, we compute reference CTs from another, smaller dataset which can be assumed to cover similar variations, and then assign each of the SMHI-LENS fields to one of these CTs. The other dataset is chosen to obviate the task of smartly selecting the SMHI-LENS SLP fields that would result in a representative set of CTs that accounts for trends between the different periods, variability over the year and between ensemble members. This dataset contains regional climate model simulations with the HCLIM38-ALADIN model (Belušić et al. 2020) over a pan-Scandinavian domain forced with two GCMs that have a considerably different forced response over the domain (EC-Earth and GFDL, Lind et al. 2022) and can be interpreted as two members of an ensemble simulation, equivalent to parts of the ensemble spread in SMHI-LENS. The total of 120 years of daily year-round data are used from the historical, mid- and end of the twenty-first century periods (Lind et al. 2022), hence covering the time span also analyzed in SMHI-LENS. The spatial mean is removed from each field before the classification, following the argumentation and procedure in Hansen and Belušić (2021).

The choice of the reference CTs does not considerably affect the results of the analysis. For example, the 10 reference CTs computed from 20 years of the ERA5 reanalysis data (Hersbach et al. 2020) could have been used too, since they strongly resemble the current CTs (compare Fig. 2 to Supplementary Figure S1), although their relative frequencies are slightly different. However, since the ERA5 CTs cover the present climate only and hence miss one important factor of variability from this study, the future evolution of the climate, we decided against this. The similarity between the present-day ERA5 CTs and the scenario CTs points to a potential invariance of CTs with future climate change, which will be explored further below. Finally, with the resulting 10 SLP CTs being clearly distinct from each other (see Fig. 2), the assignment of the SMHI-LENS SLP fields is considered to be insensitive to the choice of any of these sets of representative CTs.

Each daily SLP spatial anomaly field of the SMHI-LENS is then assigned to one of the 10 reference CTs by measuring

the similarity between the field and each CT as the Euclidean distance between them. In the resulting classification catalogue (the time series of CT numbers) the day is given the number of that CT which has the smallest Euclidean distance to the SLP spatial anomaly field of that day. SMHI-LENS CTs are then computed afterwards as averages over all members of one class, i.e. all days with the same number in the classification catalogue.

We compute frequencies of the 10 CTs separately for three 20-year periods representing the historical period (1995–2014), the middle (2041–2060) and the end (2081–2100) of the twenty-first century. Individual months are analysed as well as individual scenarios, both in terms of averages expressed through ensemble means, and spread expressed through ensemble standard deviations. When the frequency changes between different periods are analysed, there are different ways of addressing their significance. A common way of quantifying statistical significance is to use the Student's t-test (Wilks 2011). Applying the Student's t-test to SMHI-LENS resulted, however, in most changes being significant at the 99% level (not shown) which can be explained by the relatively large number of ensemble members decreasing the t-test's significance threshold. We hence use a more conservative significance test to allow interpretation of the most interesting changes. Unlike statistical significance, which generally increases with the sample size, practical significance can be defined as a "signal" that exceeds some "noise", where both signal and noise have to be further specified. In our study, we define the signal to be the ensemble mean of a change, such as the change in CT frequency between the middle or the end of the twenty-first century in a specific scenario and the historical period:

$$S = \frac{1}{M}\sum_{i=1}^{M}\left(\Phi_i^{\mathrm{F}} - \Phi_i^{\mathrm{P}}\right) \tag{1}$$

where S denotes the signal, ϕ the CT frequency (or another variable, see below), F and P future and present climate, respectively, i the individual ensemble members and M the total number of ensemble members, i.e. 50. Noise in this study is defined as the internal variability of the model, which is quantified as one standard deviation across the 50 ensemble members in the 20-year historical period:

$$N = \sqrt{\frac{1}{M}\sum_{i=1}^{M}\left(\Phi_i^{\mathrm{P}} - \overline{\Phi^{\mathrm{P}}}\right)^2} \tag{2}$$

where N denotes the noise and overbar the present-climate ensemble mean.

As a result of this definition, our results are not overly sensitive to the number of ensemble members. Our results are also not sensitive to the choice of period used to define the internal variability; the ensemble standard deviation of CT frequency does not change notably from the historical to any of the analyzed future periods.

By defining the significance of a change in the way as is done here, that is when $S/N > 1$ (as also in, e.g., Chapman and Walsh 2007; Christensen et al. 2007; however with different significant thresholds), a significant change in the mean CT frequency implies that the mean CT frequency in the future climate lies outside the most likely range of CT frequencies in the present climate. This is slightly different to the interpretation of significance as used, e.g., in Wyser et al. (2021) who relate the ensemble mean of the change signals of the 50 members (e.g. temperature change from historical to mid century in a scenario) to the ensemble standard deviation of changes. If this ratio is larger than 2, one can say that 97% of all members agree on the signal, which can, however, also be a small change of no practical significance.

2.3 Effect of circulation types on dependent variables

Each CT is associated with a specific response in the local weather and climate, which can be different for each month and change over time. In this study, we call the response in surface temperatures (TAS) and precipitation (PR) the "effect" that the CT has on these variables. We express the effect as anomalies from the climatological seasonal cycle ($\mathrm{TAS_{anom}}$ and $\mathrm{PR_{anom}}$, respectively) to see whether the occurrence of a specific CT is linked to colder or warmer temperatures than would normally occur, and to more or less precipitation.

With the climate changing globally, the effect of the CTs on TAS and PR could also be changing. Each of the 10 CTs that are computed in this study can undergo differently pronounced changes in each calendar month and each scenario. As it is impossible to present spatial maps for each of these cases for the two variables of interest, we compute and compare two measures for each of these fields: (1) the spatial extent of the significant CT effect changes, expressed as the percentage of significantly changing grid points in the domain, and (2) the magnitude of the CT effect changes, expressed as the sum of the absolute changes at significant grid points. Significant changes are defined as outlined above for CT frequency as exceedances of the internal variability of the model, which again is defined as the ensemble spread (one standard deviation) of CT effect in the 20-year period of the historical simulation. In other words, in Eqs. 1 and 2, ϕ denotes $\mathrm{TAS_{anom}}$ and $\mathrm{PR_{anom}}$.

To indicate the direction of the CT effect change, i.e. whether the CT effect on temperature and precipitation is strengthening or weakening in the future climate, we first compute at each grid point the difference between the future

and present climate CT effect fields and multiply it by the sign of the effect in the present climate at that grid point. We found that the sign of the sum over all significantly changing grid points is then a good indicator of the predominant direction of the CT effect change in the whole domain.

3 Results

3.1 Circulation type spatial patterns

The mean climate flow over the pan-Scandinavian domain is dominantly westerly and varies slightly around this direction over the year. During autumn, winter and spring, the flow direction is mainly south-westerly, while in summer, it changes towards westerly or north-westerly. The SLP magnitudes are generally higher during summer than during winter, while SLP gradients are strongest in winter, especially along the mountain chain at the Norwegian west coast (Figure S2; see also Lind et al. 2020; Kjellström et al. 2022). The CTC using the SANDRA algorithm splits up this mean SLP climate into the most dominant representative circulation patterns. Figures 2a and 3a show the characteristics of the 10 SLP CTs in the historical 20-year period (1995-2014), together with their effect on TAS (Fig. 2a) and PR (Fig. 3a). Note that the results are based on the year-round data, without a-priori separation into individual seasons. The CTs are sorted by their number of members with CT1 being the largest, i.e. occurring most often during that period and accumulated over all 50 SMHI-LENS ensemble members, and CT10 being the smallest.

The most frequent CT (CT1) shows a high-pressure ridge extending over Scandinavia and Finland associated with weak winds and generally no strong TAS and PR anomalies. The TAS effect is, however, different in individual seasons, where the CT1 SLP pattern is associated with colder than normal temperatures in winter and warmer than normal temperatures in summer (not shown). Other CTs also show some variation of their TAS or PR effect over the year, but those are usually not changing signs as for TAS in CT1 and will therefore not be discussed in detail here.

CTs where the flow has a northerly or easterly component over the Scandinavian land masses are generally associated with colder than normal temperatures in this region (CT3, CT4, CT6), with strongest negative TAS anomalies of up to − 1.5 K occurring in CT6 situations. On the other hand, when the flow is more from the south or the west as in CT5, CT7, CT8, CT9 and CT10, temperatures are generally warmer than normal. Strongest positive TAS anomalies over Scandinavia of up to + 2 K are associated with CT10, a westerly SLP pattern with a strong pressure gradient and hence strong winds.

CT10 also has the largest effect on precipitation, where the strong westerly winds impinging on the Scandes induce anomalies of up to 14 mm/day. As expected, the flow towards the mountains from the different directions is mainly dominating the PR effects of the CTs, leading to wetter-than-normal conditions upstream and drier-than-normal conditions downstream of the mountains. Driest conditions over southern Scandinavia are associated with CT4 and CT5 patterns, and over the Scandes and northern Scandinavia with CT1, CT3 and CT6.

Regarding the changes in the year-round SLP patterns of the 10 CTs towards the end of the 21st century, they generally have maximum values on the order of 1 hPa and are hence relatively small. This can be seen from the comparison of panels a and b in Figs. 2 and 3, and also Figure S4 showing the differences between historical and end-century CTs of the strongest SSP585 scenario as an example. Largest SLP changes occur in CT5 as a decrease centered over southern Sweden and the northeastern Baltic Sea. The largest relative SLP gradient change occurs in CT3, with the future decrease of the domain-wide gradient of about 14% in SSP585. Apart from that, the CTs do not experience a considerable change in their SLP patterns or gradients in the future climate (the next largest gradient change is the decrease of about 6% in CT4 in SSP585, while for all the other CTs the gradient change is less than 2%). The future change in the effects of CTs on TAS and PR will be discussed in Sect. 3.3.

3.2 Circulation type frequencies

The average SLP patterns change over the different seasons, mainly in terms of the SLP magnitude and gradient, and somewhat with regard to the spatial pattern orientation, i.e. flow direction (Figure S2). Since in this study the CTC was performed on all the seasons together, the SLP seasonal change is predominantly expressed as the seasonal variability of the frequency of the individual CTs (Fig. 4, upper panel). CTs 1–4 occur most often between May and August, with each of them peaking in one of these months. Their frequencies are considerably higher than those of the other CTs in these months and decrease towards winter, where they are then lower than most of the other CTs. Hence, CTs 1–4 can be regarded as summer-CTs. On the other hand, CTs 7–10 have their maxima in winter and minima in summer and can hence be called winter CTs. Note that the seasonal amplitude of the winter-CTs is smaller than that of the summer-CTs because all CTs have some occurrences in the winter months while it is basically only the four summer-CTs occurring in summer. CT5 and CT6 peak in the transition seasons, with CT5 appearing as the autumn-CT and CT6 as the spring-CT.

To analyse CT frequency changes towards the middle and the end of the twenty-first century in SMHI-LENS, we start

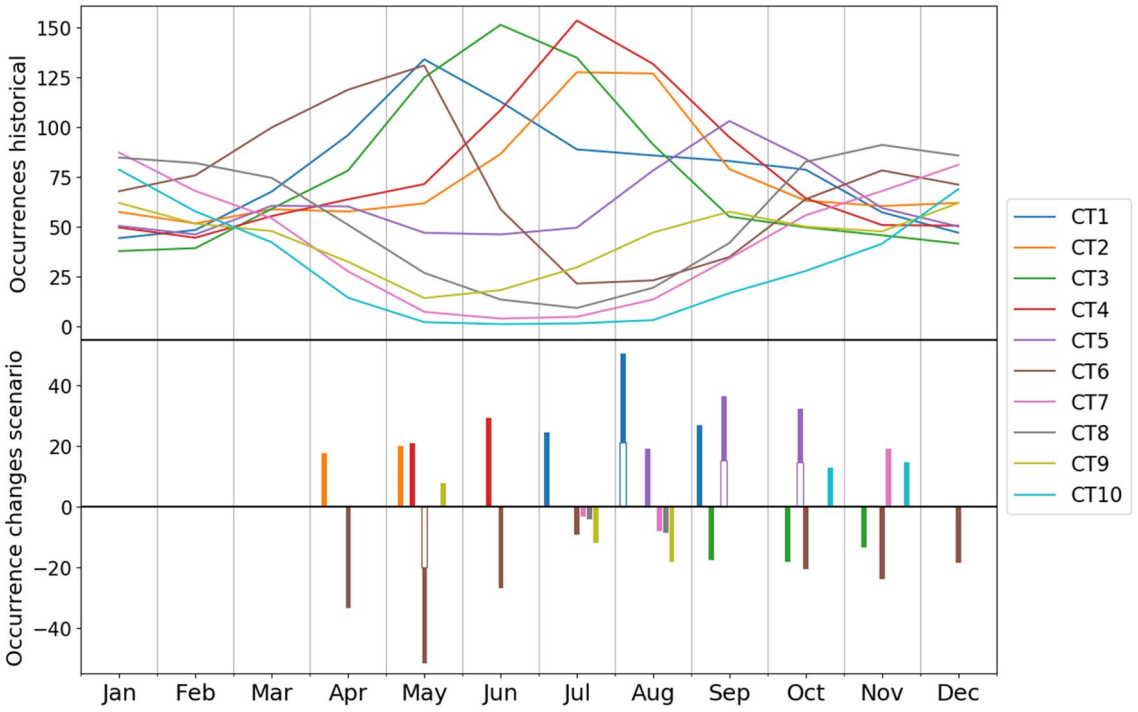

Fig. 4 Upper panel: total number of occurrences of each CT in each month. Shown is the ensemble mean of 50 members from 20 years of the historical simulation (1995–2014). Lower panel: significant 20-year occurrence changes from the historical towards the middle (2041–2060; unfilled bars) and the end (2081–2100; filled bars, starting at zero) of the twenty-first century in the SSP585 scenario

with looking at the changes in the SSP585 scenario which, of all the scenarios, shows the strongest global warming signal. A generalization of SSP585 findings to all scenarios is done afterwards.

Significant CT frequency changes in the SSP585 scenario towards the middle and the end of the twenty-first century are shown in the lower panel of Fig. 4 for all individual months. As described in Sect. 2.2, significance is defined when the scenario ensemble mean change signal between the future 20-year period average and the historical 20-year period average exceeds one standard deviation of the ensemble spread spanned in the historical period. Only a few CTs show a significant frequency change towards the middle of the twenty-first century (unfilled bars): CT6 frequency decreases in May, CT1 frequency increases in August as does CT5 frequency in September and October. Towards the end of the twenty-first century (filled bars), three of the four summer-CTs become more frequent between April and September. More specifically, it is the late-summer-CTs 2 and 4 that increase in frequency in late spring and early summer, and the early-summer-CT1 whose frequency increases in mid and late summer. At the same time, the spring-CT (CT6) becomes less frequent between April and July which altogether could indicate more summerlike conditions in the future under SSP585, or at least a clearer distinction between summer and winter in terms of CTs. This is supported by the frequency decrease of winter-CTs 7–9 in July and August. The increase in the autumn-CT5 in September and October is one of the few changes already significant towards the mid-century. It is partly counteracted by a decrease in summer-CT3 and spring-CT6, again suggesting a clearer separation between the seasons. In November, CTs 7 and 10 become more frequent while CTs 3 and 6 occur less often. No significant frequency changes occur in any of the CTs between January and March.

Figures equivalent to the lower part of Fig. 4 but for the five other scenarios can be found in Supplementary Figure S3. To generalize the results for all the scenarios, Fig. 5 summarizes how many of the overall six scenarios show significant frequency changes for the individual CTs and in the individual months towards the middle (Fig. 5a) and the end (Fig. 5b) of the twenty-first century. The general picture drawn above from the SSP585 scenario is confirmed here. For the mid-century period, only the significant frequency decrease in CT6 in May is found in two other scenarios as well (SSP534OS and SSP434); the other significant changes seen in Fig. 4 are constricted to SSP585 only. For the end of the century period, the results from all scenarios confirm the SSP585 result that most of the significant frequency changes are projected for the summer half-year, with 55 out of the

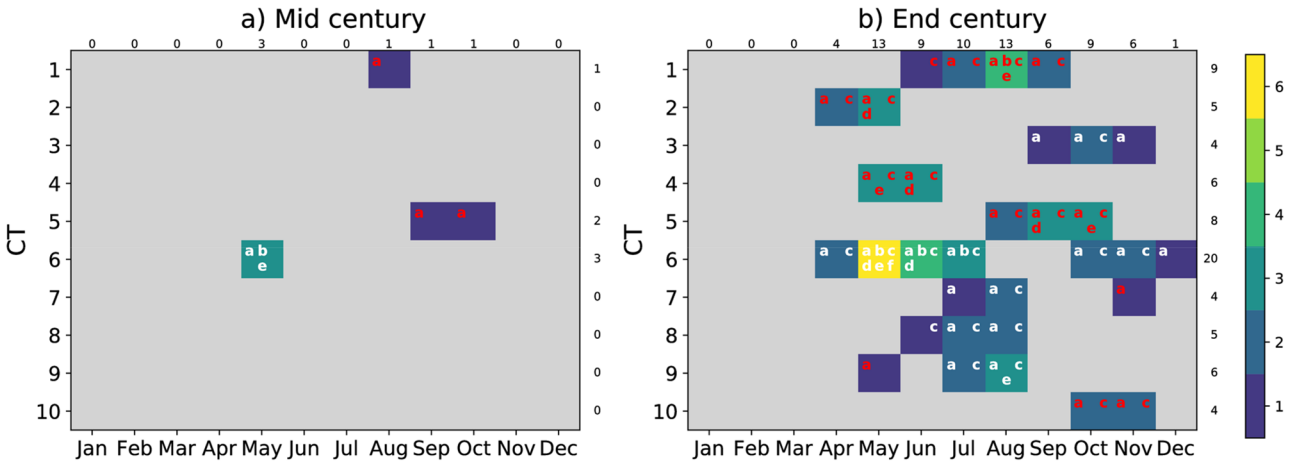

Fig. 5 Number of scenarios that show a significant CT frequency change from the historical period towards **a** the middle and **b** the end of the twenty-first century. Gray indicates no significant change in any of the scenarios. Each cell represents one CT and month, and the letters indicate whether the frequency increases (red font color) or decreases (white font color) in an individual scenario: **a** SSP585, **b** SSP534OS, **c** SSP370, **d** SSP245, **e** SSP434, **f** SSP119. The cell color indicates the number of scenarios with significant change (depicted also by the number of letters). The numbers to the right of each subfigure give the total number of significantly changing scenarios for each CT (maximum is 12 months × 6 scenarios = 72); the numbers above each subfigure give the total number of significantly changing scenarios for each month (maximum is 10 circulation types × 6 scenarios = 60)

overall 71 significantly changing CT/scenario combinations occurring between April and September (compare top row numbers in Fig. 5b). Of all the CTs, CT6 shows most significant frequency changes accumulated over all scenarios and months (20 out of 72 possible month/scenario combinations), having a general decrease whenever significant changes occur (indicated by the minus signs in the respective boxes). The frequency decrease seen for CT6 in May is the only case where all six scenarios indicate a significant change. This decrease is also in line with the projected frequency decrease of a comparable CT computed over a larger, European domain in a recent study by Røste and Landgren (2022; see their CT8), shown for summer months towards the end of the twenty-first century in some Euro-CORDEX models.

In general, there is consistency between the scenarios in terms of the direction of frequency change; there is not a single CT or month with both decrease and increase projected from different scenarios. Furthermore, the projected CT frequency changes tend to follow the strength of the projected global warming changes in the scenarios such that most significant CT frequency changes towards the end of the twenty-first century are seen in the strongest scenarios (SSP585 and SSP370) and fewest in the weakest scenario (SSP119). The significant CT frequency changes of the other scenarios that lie in between (SSP245, SSP534_OS and SSP434) are however not strictly sorted according to their warming signal.

3.3 Effect on temperature and precipitation

The second aspect of future changes related to CTs is that of the potentially changing effect that the CTs have on the local weather and climate. It is cumbersome to present spatial maps of changes for each of the 10 CTs in each of the 12 months, for all six scenarios in both future periods considered and the two variables of interest, surface temperature and precipitation. Maps showing the end of century year-round CT effect on TAS and PR are exemplarily shown for the SSP585 scenario in Figs. 2b and 3b. In the following, the results are summarized for all scenarios in a similar way as in Sect. 3.2.

One way to analyze and summarize future changes of generally very different spatial patterns such as the 10 CTs and their individual peculiarities in the different months is to look at their spatial extent. To do that, we count how many grid points in our domain of interest experience a significant CT effect change. Significance of a change is again defined as the exceedance of one standard deviation of the ensemble spread in the historical period. This number (as a percentage of grid points) is computed for each ensemble member in each scenario separately, and Fig. 6 presents the averages over all scenarios and ensemble members for each CT and month for both future periods. The results are insensitive to averaging over land points only (not shown).

The effect that the CTs have on TAS does not change on a larger scale towards the middle of the twenty-first

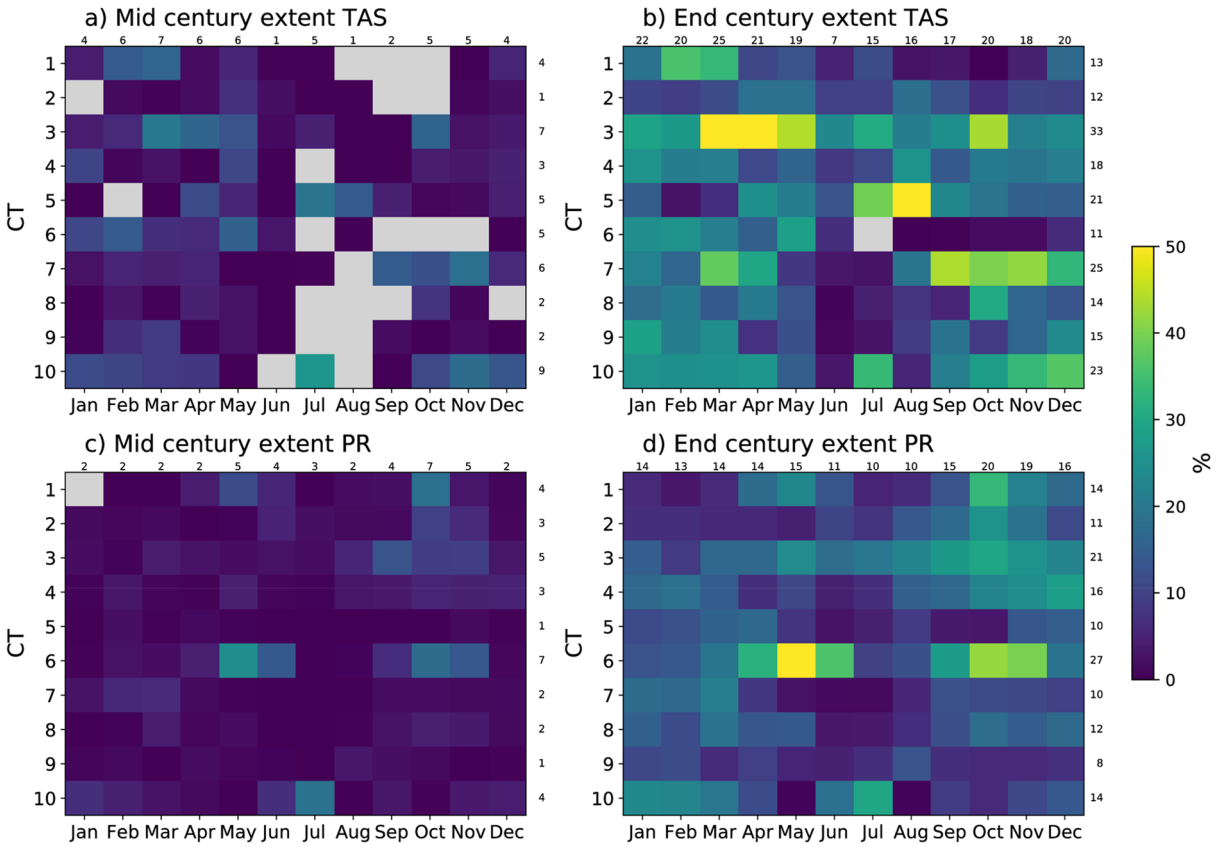

Fig. 6 Spatial extent of significant CT effect changes for each CT and month, shown as the percentage of grid points that experience a significant change from the historical period towards the middle (left) and the end (right) of the twenty-first century, for TAS (top) and PR (bottom). Gray denotes no significant changes. The numbers to the right of each subfigure are the averages over the respective rows (i.e. CTs); the numbers above each subfigure are the averages over the respective columns (i.e. months). All six scenarios are considered

century (Fig. 6a). Significant changes become more spatially extended towards the end of century (Fig. 6b), when scenario averages show significant CT TAS alterations over more than half of the domain in individual months and CTs. Largest-scale changes are projected for CT3, a low-pressure system located over the southeast of the domain which of all CTs is showing the largest relative SLP gradient decrease (see Sect. 3.1). CT3 is associated with north-easterly winds over Scandinavia and lower-than-normal temperatures. CT3 TAS effect changes are most spatially pronounced in spring between March and May and in October. Figure 7a, which shows the map of these CT3 TAS effect changes exemplarily for the SSP585 scenario in April, reveals that the cooling effect that CT3 has on TAS in the historical climate (cf. Fig. 2) is significantly reduced towards the end of the twenty-first century over large parts of the domain. This general CT3 TAS effect change signal is seen in all individual months.

Similar large-scale TAS effect changes are also projected for CT5 in July and August as well as CT7 between September and November. The CT5 TAS effect change occurs as a large-scale cooling tendency, i.e. a reduction of the present-day warming effect, as shown in Fig. 7b. In general, there is a tendency for the TAS effect changes of the winter-CTs (CTs 7–10) to be of smaller spatial extent in the summer months. CT6, which was shown to be outstanding in terms of significant CT frequency changes (see Sect. 3.2), shows fewest significantly changing grid points for its effect on TAS.

For the changes in the CT effect on precipitation, however, it is again CT6 which is showing the strongest signal. Especially in May, where all six scenarios are showing a significant frequency decrease (Fig. 5), CT6 has a significantly different effect on PR in more than half of the domain towards the end of the twenty-first century (Fig. 6d). The changing pattern consists of a wettening in the southwestern corner of the domain and a drying above the Scandes extending over Finland (Fig. 7c) and can be seen in all months. Otherwise, the spatial extent of significant CT PR effect changes is generally smaller than for temperature. Further noticeable are the relatively large-scale changes of the summer-CTs (CTs 1–4) in autumn and partly early winter.

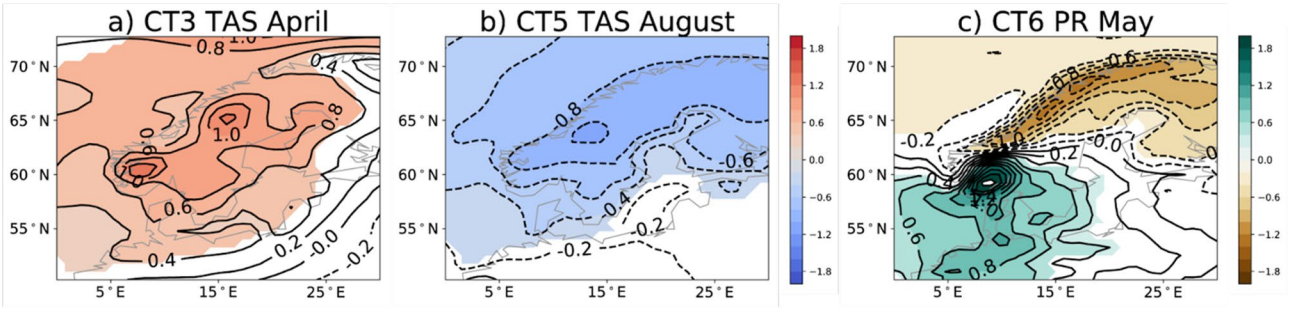

Fig. 7 Example maps of interesting cases for the change of a CT's effect on TAS or PR as identified from Figs. 6 and 8. The fields show the ensemble mean change in the SSP585 scenario from the historical period to the end of the twenty-first century. Colours indicate significant signals as defined in Sect. 2.2. **a** CT3 TAS effect change in April (in K); **b** CT5 TAS effect change in August (in K); **c** CT6 PR effect change in May (in mm/day)

A second way of analysing the CT effect changes for TAS and PR is to look at the strength of the significant changes. The results are presented in Fig. 8 which shows the sum of the magnitudes of changes at significant grid points for each CT and month. Changes can occur in both directions, towards a stronger or a weaker effect. A strengthening of the effect in this context means that a cooling or wettening effect in the present climate gets cooler or wetter in the future climate, and a warming or drying effect gets warmer or drier. Changes can further occur in different ensemble members, the different scenarios and in different locations of the same field and could partly cancel out when the sum

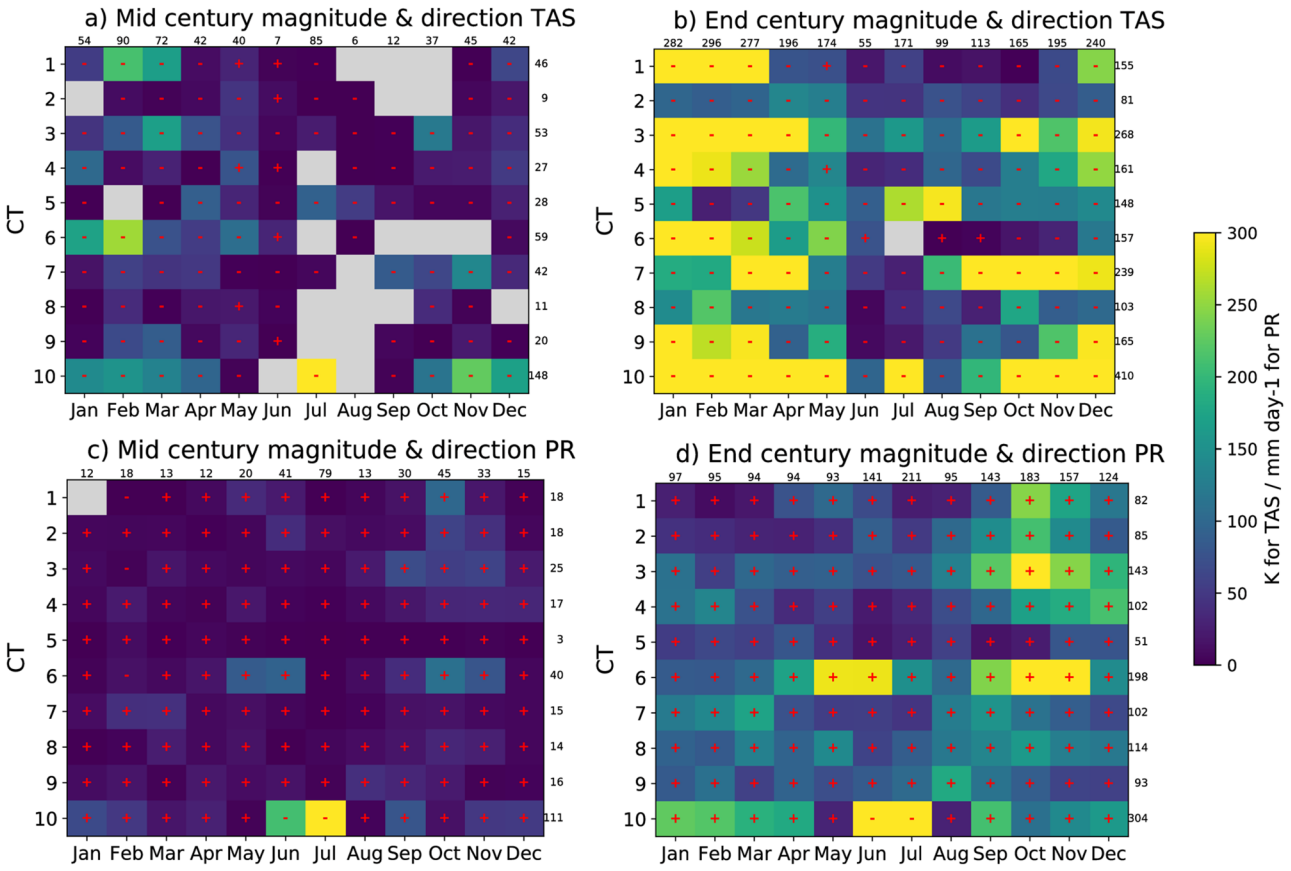

Fig. 8 As Fig. 6, but for the magnitude of significant CT effect changes in each CT and month, shown as the sum of the absolute changes at all significantly changing grid points. "+" and "−" signs indicate whether the effect is strengthening or weakening compared to the historical period

over all these aspects of variability is computed. Because of that, sums of the absolute values of changes are considered for Fig. 8. To additionally indicate whether the effect of the CTs on TAS and PR is strengthening or weakening in the future periods, "+" and "−" signs denote the direction of the change in the individual months with respect to the historical period, and are calculated as described in Sect. 2.3. A "+" sign hence indicates that a present climate warming or wetting CT effect is getting warmer or wetter in future climate, or that a present climate cooling or drying effect is getting cooler or drier. A "−" sign denotes that a warming, cooling, wetting or drying is reduced in the future.

The strength of change as computed here is by construction closely related to the spatial extent analysed above. A comparison with a different approach, depicting the strength as the average over all (absolute or raw) values at significant grid points instead of the sum, generally revealed the same overall picture as described in the following, but misleadingly emphasized fields with few strongly changing grid points.

Remarkably, apart from a few exceptions, the effect that the individual CTs have on temperature, independent of whether this effect is a warming or a cooling in the historical period, weakens towards both future periods in all months, as indicated by the predominant "−" signs in Figs. 8a, b. This weakening can also be seen from the exemplary maps showing the year-round future CT effect on TAS for the SSP585 scenario in Figure S4 in comparison to Fig. 2a. This means that in many regions which experience a warming effect of a CT in present climate, this warming is reduced in future climate, and a present climate cooling effect is getting less cool towards the end of the twenty-first century. The general weakening of the TAS effect can also be seen as a general weakening of differences between the individual CTs with regard to their TAS effect (compare Fig. 2a, b). We found that this weakening is consistent with a decreasing interannual variability in the future scenarios (not shown, but adumbrated in Fig. 1). What we call the effect of a CT is the averaged anomaly of all days experiencing that CT, with the anomaly being defined at each grid point as the deviation from the climatological daily annual cycle in the specific period we are looking at (historical or one of the future periods). If the interannual variability decreases, the anomalies are generally smaller deviations from the mean, in both directions, positive and negative, in the future period.

Figure 8 suggests that the weakening of the CTs' effect on TAS is generally strongest in winter and early spring for a large number of CTs, and weakest in summer. This tendency is already indicated towards the mid-century future period (Fig. 8a) and becomes even more pronounced towards the end-century period (Fig. 8b). Large changes are again seen in CT3, one of the "summer clusters" that is projected to decrease strongest in its SLP gradient (see above) and is associated with a north-easterly flow towards Scandinavia and lower-than-normal temperatures. Given the comparatively low frequency of occurrence of CT3 in winter, these strong changes are presumably of minor importance for the overall future temperature conditions; however, their importance could increase substantially in April where CT3 is the third most frequent circulation type. Strong changes are further seen in the autumn to early spring TAS effect of CT7, a "winter-cluster" associated with above-normal temperatures over the whole domain, and CT10.

A similar systematic change as for TAS is projected for the effect that the CTs have on PR, although of the opposite sign. Here, with even less exceptions, a systematic strengthening of the effect is seen in Fig. 8c, d. This means that those CTs which are associated with above-average precipitation in the historical period could be associated with even higher positive PR anomalies. The historically "dry" CTs could become even drier, although in absolute terms most of the "dry" CTs are simply CTs with little to no precipitation which cannot be reduced further. The systematic strengthening of the CTs' effect on PR can be explained with an increased interannual variability in precipitation in the future climate, following the same argumentation as above for temperature. It also means that the differences between the individual CTs' PR effect is enhanced in the future climate.

Figure 8c, d suggest that strongest changes for the PR effect occur between September and December, although the systematic differences between the individual months and seasons are less pronounced than for TAS. Changes in these months are also dominated by changes of the less-frequent CTs 1–4 and hence of minor importance. When comparing the effect change of the individual CTs, CT6 shows the strongest signals: its effect on PR, which involves wetter-than-normal conditions over southern Scandinavia and drier-than-normal conditions west of the Scandes due to an easterly-dominated flow over the domain, becomes substantially stronger especially in May—CT6's peak month of occurrence, June, October and November (compare Fig. 7c).

While the analysis above (Figs. 6, 8) summarizes the results for all six scenarios, the SMHI-LENS provides the unique opportunity to investigate the uncertainties in future changes that are due to uncertainties in external forcings, like emissions of greenhouse gases and other socio-economic developments. We therefore investigated the spatial extent and the magnitude of the changes of the effect that the CTs have on TAS and PR in each individual SSP scenario. In general, the strength of the CT-related changes increases linearly with the strength of the scenarios—the stronger the scenario in terms of warming signal (globally and over the pan-Scandinavian domain considered here), the stronger the change in CT. Comparing the behavior between the scenarios and the two future periods, the strength of the respective changes follows the following order for the vast majority of

CTs and months, and for both TAS and PR: the end-century change of the weakest scenario SSP119 is exceeded already by the mid-century change of all other scenarios, and all but the weak SSP119 scenario show stronger changes towards the end-century than the strongest scenario SSP585 towards the mid-century (not shown). This is consistently following the general warming tendencies over the domain and the precipitation changes in the different scenarios (Fig. 1a, b).

4 Summary and discussion

The large-scale atmospheric circulation affects the local weather and climate by linking, e.g., the large-scale pressure structure to local surface temperature and precipitation. The question addressed in this study is whether and how climate change affects the large-scale atmospheric circulation and its effect on surface parameters. Potential changes in the large-scale circulation could alter the expected thermodynamic changes and have implications for relevant scientific applications like the assessment of future regional climate changes through statistical downscaling of large-scale patterns.

Assessment of the future climate requires some estimation of the uncertainty, and this study addresses parts of this uncertainty using the unique dataset provided by the SMHI large ensemble (SMHI-LENS). We analyze three 20-year periods, one representing the present climate (1995–2014) and two for the middle and the end of the twenty-first century (2041–2060 and 2081–2100). Six different future SSP scenarios are analyzed to estimate uncertainties resulting from external forcings like the emission of greenhouse gases and other socio-economic developments. Each SMHI-LENS scenario alone with its 50 members includes the general advantages of single-model initial-condition large ensembles such as the ability to quantify and separate a climate signal from internal variability (e.g. Maher et al. 2021). Having available six scenarios with 50 ensemble members allows for addressing an additional uncertainty factor – one that is stemming from external forcings—and hence makes SMHI-LENS an ideal testbed to obtain robust results.

This article focuses on a pan-Scandinavian domain where the general flow direction is westerly, with generally higher absolute pressure during summer and a stronger pressure gradient during winter. To answer the question given above, this study splits up the mean SLP climate and expresses the large-scale atmospheric circulation using sea level pressure circulation types (CTs), which are representative dynamical situations computed using the circulation type classification method SANDRA. We investigate how the frequency of the ten prevalent CTs changes from present to future climate as well as the effect that these CTs have on temperature and precipitation over the domain of interest. We also address the seasonal variations of CTs and their changes. The significant future change in the characteristics or effects of CTs is determined as a change that exceeds the present-day ensemble variability.

The analysis reveals the following:

- CTs affect surface temperature and precipitation in accordance with their sea level pressure patterns. The general characteristics and effects of the individual CTs are mostly stable over the annual cycle with few exceptions, e.g. high-pressure systems being linked to surface cooling in winter and surface warming in summer.
- The frequency of occurrence of the individual CTs is highly variable over the year. Of the ten prevailing CTs, four can be regarded as summer CTs, four as winter CTs, and two are dominating one of the two transition seasons.
- Significant changes in the CT frequency towards the middle of the twenty-first century are limited to a few individual CTs and months and are mainly found in the strongest considered scenario simulation (SSP585). Towards the end of the twenty-first century, changes in CT frequency suggest an extension of summer conditions towards spring and autumn and point towards a clearer distinction between summer and winter: three of the four summer-CTs become more frequent in late spring and early autumn, while the spring-CT as well as three of the four winter-CTs become less frequent in individual summer months. No significant CT frequency changes occur during winter months.
- Similarly to the CT frequency changes, the effect of the CTs on surface temperature and precipitation changes significantly mainly towards the end of the twenty-first century. A clear weakening of the CTs' effect on temperature is found for all CTs and all months, i.e. independent of whether the CT is associated with generally warmer- or colder-than-normal conditions. This also means that the difference between the individual CTs' effect on temperature is suppressed in a warmer climate. Conversely, for precipitation a strengthening of the CT effect is found, also consistent over all CTs and months, resulting in the difference between the CTs' effect on precipitation being enhanced. The changes in the CT effect on temperature are strongest during winter and early spring, while for precipitation, they are strongest between September and December.
- Largest-scale and strongest changes in the CT effect on temperature are found for CT3, a low-pressure system located towards the southeast of the domain. Its association with lower-than-normal temperatures is suppressed significantly over large parts of the domain towards the end of the twenty-first century in all months, especially between March and May and in October. For the CTs' effect on precipitation, largest-scale and strongest changes are projected for CT6. CT6 involves a wetten-

ing over Southern Scandinavia and a drying west of the Scandes which we find significantly enhanced under future climate change in early summer and autumn.

In general, for both CT frequency and their effect on the surface variables, the projected changes roughly follow the strength of the scenarios' projected warming trends and are most pronounced in the SSP585 scenario.

We find that the general weakening of the CT effect on surface temperatures is related to a general decrease in interannual temperature variability towards the end of the twenty-first century in SMHI-LENS. A similar decrease can also be seen in Bathiany et al. (2018; cf. their Fig. 1c) for northern and middle Europe with a high consistency throughout various CMIP5 models. Reasons for the decreasing interannual temperature variability are suggested to lie in a reduction of the meridional temperature gradient that goes along with Arctic amplification under future global warming (Screen 2014; Holmes et al. 2016; Schneider et al. 2015; Bathiany et al. 2018). The decrease in temperature variability is consistent with smaller anomalies with respect to the future mean state in temperature and hence with a weakened effect of the circulation on temperature. The future temperature distributions in our domain of interest do not only decrease in variance, but also the skewness becomes less negative (not shown), indicating stronger warming of the cooler part of the distribution. For precipitation, SMHI-LENS projects a general increase of the interannual variability which is consistent with the strengthening of the CT effect described above. With precipitation being restricted at the lower end of the distribution by dry days, this strengthening effectively means that those CTs which are associated with wetter-than-normal conditions in the present climate will be associated with even more precipitation in the future. The latter is consistent with the future increase in mean precipitation and also with the humidity, and consequently extreme precipitation, increasing with temperature according to the Clausius-Clapeyron scaling (e.g. Pall et al. 2007; O'Gorman and Schneider 2009).

During the review process of this study, an article from Mittermeier et al. (2022) was published that analyzed, among other questions, CT frequency changes in the SMHI-LENS SSP370 scenario over a large Europe-North Atlantic domain. Their results are consistent with our finding that the frequency of some CTs changes significantly under future climate change. Details, however, differ from their as well as from other studies that analyze future circulation changes. For example, Huguenin et al. (2020) find no change in any summer and winter CT frequencies towards the end of the twenty-first century, but their focus is on Central Europe and, probably more important in this context, they use a different classification method, namely the Grosswettertypes (GWT) classification method which was also applied in Mittermeier et al. (2022). GWT groups the large-scale pressure fields mainly based on their predominant flow direction and basically does not take into account the pressure gradient magnitude which limits its efficacy in separating effects of CTs on other variables such as temperature and precipitation (Hansen and Belušić 2021). Therefore the CTs in Huguenin et al. (2020) have different characteristics than the CTs in this study classified using the SANDRA method [see Hansen and Belušić (2021) for a comparison between GWT and SANDRA CTs]. Further, Stryhal and Huth (2019a, b) find a significant increase in westerly flow types during winter, which seems not to be in line with the results from Huguenin et al. (2020) nor this study. Our analysis shows no CT frequency changes in winter, but indicates significant changes in the summer and partly spring and autumn such that a clearer separation between the seasons and more summer-like conditions emerge in the future climate. This apparent contradiction between different studies indicates the existing uncertainties associated with analyses of future projections in general, and those of future CT changes specifically. We postulate that SMHI-LENS with its large amount of realizations for both the present and several potential future climates addresses many of the previous uncertainties in one and the same testbed and allows us to obtain statistically robust results for the assessment of future CT changes.

Frequency changes of specific CTs could imply changes in extreme events. For example, heatwaves over Scandinavia are often associated with persistent blocking situations which correspond to the CT1 in our study. In fact, the extreme heatwave in summer 2018 which had devastating impacts on different sectors of society (Wilcke et al. 2020) had one third of all days between May and July assigned to the CT1 equivalent in a set of 10 CTs obtained from ERA5 reanalysis (Hersbach et al. 2020) using SANDRA (not shown). Our analysis revealed a significant increase in CT1 frequency during summer and hence indicates that heatwaves will become more frequent over Scandinavia. Further analysis about the connection between CTs and extreme events in SMHI-LENS is ongoing and will be presented in a separate study.

Supplementary Information The online version contains supplementary material available at https://doi.org/10.1007/s00382-023-06704-y.

Acknowledgements EU COST Action 733 is acknowledged for producing and making available the classification software. The computations for SMHI-LENS were enabled by resources provided by the Swedish National Infrastructure for Computing (SNIC), partially funded by the Swedish Research Council through Grant agreement no. 2018-05973.

Author contributions FH and DB developed the conception and design of this study. FH prepared the figures and wrote the first draft of the manuscript. KW performed the SMHI-LENS simulations. All authors contributed to the discussion of the results and commented on the manuscript.

Funding Open Access funding enabled and organized by Projekt DEAL. This study received support from the EU Horizon 2020 EUCP project (grant no. 776613), the Formas EDUCAS project (Grant no. 2019-00829) and the EU Horizon 2020 Project "CLIMATE INTELLIGENCE Extreme events detection, attribution and adaptation design using machine learning (CLINT)" (Ref: 101003876-CLINT).

Data availability All results from SMHI-LENS are available from any ESGF data node as part of CMIP6; search for <model_id> EC-Earth3 and <variant_label> in the range r101i1p1f1 and r150i1p1f1.

Declarations

Conflict of interest The authors declare no competing interests.

References

Baldwin MP et al (2001) The quasi-biennial oscillation. Rev Geophys 39:179–229. https://doi.org/10.1029/1999RG000073

Bathiany S et al (2018) Climate models predict increasing temperature variability in poor countries. Sci Adv 4:eaar5809

Beck C, Philipp A (2010) Evaluation and comparison of circulation type classifications for the European domain. Phys Chem Earth 35(9–12):374–387

Beck C et al (2007) Frequency and within-type variations of large-scale circulation types and their effects on low-frequency climate variability in Central Europe since 1780. Int J Climatol 27(4):473–491. https://doi.org/10.1002/joc.1410

Belušić D et al (2020) HCLIM38: a flexible regional climate model applicable for different climate zones from coarse to convection-permitting scales. Geosci Model Dev 13:1311–1333. https://doi.org/10.5194/gmd-13-1311-2020

Cahynova M, Huth R (2016) Atmospheric circulation influence on climatic trends in Europe: an analysis of circulation type classifications from the COST733 catalogue. Int J Climatol 36:2743–2760. https://doi.org/10.1002/joc.4003

Cattiaux JA et al (2010) Winter 2010 in Europe: a cold extreme in a warming climate. Geophys Res Lett 37:L20704. https://doi.org/10.1029/2010GL044613

Chapman WL, Walsh JE (2007) Simulations of arctic temperature and pressure by global coupled models. J Clim. https://doi.org/10.1175/JCLI4026.1

Christensen A et al (2007) Regional climate projections. In: Solomon S, Qin D, Manning M, Chen Z, Marquis M, Averyt KB, Tignor M, Miller HL (eds) Climate change 2007: the physical science basis. Contribution of working group I to the fourth assessment report of the intergovernmental panel on climate change. Cambridge University Press, Cambridge

Dai A, Blöcker CE (2019) Impacts of internal variability on temperature and precipitation trends in large ensemble simulations by two climate models. Clim Dyn 52:289–306. https://doi.org/10.1007/s00382-018-4132-4

Deser C et al (2012) Uncertainty in climate change projections: the role of internal variability. Clim Dyn 38:527–546. https://doi.org/10.1007/s00382-010-0977-x

Deser C et al (2020) Insights from Earth system model initial-condition large ensembles and future prospects. Nat Clim Change 10:277–286. https://doi.org/10.1038/s41558-020-0731-2

Döscher R et al (2022) The EC-Earth3 earth system model for the coupled model intercomparison project 6. Geosci Model Dev 15:2973–3020. https://doi.org/10.5194/gmd-15-2973-2022

Fernandez-Montes S et al (2012) Wintertime circulation types over the Iberian Peninsula: long-term variability and relationships with weather extremes. Clim Res 53(3):205–227

Fleig AK et al (2015) Attribution of European precipitation and temperature trends to changes in synoptic circulation. Hydrol Earth Syst Sci 19:3093–3107. https://doi.org/10.5194/hess-19-3093-2015

Hansen F, Belušić D (2021) Tailoring circulation type classification outcomes. Int J Climatol 41:6145–6161. https://doi.org/10.1002/joc.7171

Hersbach H et al (2020) The ERA5 global reanalysis. Q J R Meteorol Soc 146:1999–2049. https://doi.org/10.1002/qj.3803

Holmes CR et al (2016) Robust future changes in temperature variability under greenhouse gas forcing and the relationship with thermal advection. J Clim 29(6):2221–2236. https://doi.org/10.1175/JCLI-D-14-00735.1

Horton DE et al (2015) Contribution of changes in atmospheric circulation patterns to extreme temperature trends. Nature 522:465–469. https://doi.org/10.1038/nature14550

Huguenin MF et al (2020) Lack of change in the projected frequency and persistence of atmospheric circulation types over Central Europe. Geophys Res Lett. https://doi.org/10.1029/2019GL086132

Huth R et al (2007) Classifications of atmospheric circulation patterns: recent advances and applications. In: Gimeno L, GarciaHerrera R, Trigo RM (eds) Trends and directions in climate research, vol 1146. San Lorenzo de El Escorial, Spain: Annals of the New York Academy of Sciences, 7th annual meeting of the European-Meteorology-Society (EMS)/8th European conference on applications of meteorology. https://doi.org/10.1196/annals.1446.019

Ineson S, Scaife AA (2009) The role of the stratosphere in the European climate response to El Niño. Nat Geosci 2:32–36. https://doi.org/10.1038/ngeo381

IPCC (2021) Climate change 2021: the physical science basis. In: Masson-Delmotte V, Zhai P, Pirani A, Connors SL, Péan C, Berger S, Caud N, Chen Y, Goldfarb L, Gomis MI, Huang M, Leitzell K, Lonnoy E, Matthews JBR, Maycock TK, Waterfield T, Yelekçi O, Yu R, Zhou B (eds) Contribution of working group I to the sixth assessment report of the intergovernmental panel on climate change. Cambridge University Press, Cambridge. https://doi.org/10.1017/9781009157896 **(in press)**

Jacobeit J et al (2009) Central European precipitation and temperature extremes in relation to large-scale atmospheric circulation types. Meteorol Z 18:397–410. https://doi.org/10.1127/0941-2948/2009/0390

Jacobeit J et al (2017) Atmospheric circulation types and extreme areal precipitation in southern central Europe. Adv Sci Res 14:71–75. https://doi.org/10.5194/asr-14-71-2017

Jones PD, Lister DH (2009) The influence of the circulation on surface temperature and precipitation patterns over Europe. Clim past 5:259–267. https://doi.org/10.5194/cp-5-259-2009

Kjellström E et al (2022) Contributions from changing large-scale atmospheric conditions to changes in Scandinavian temperature and precipitation between two climate normals. Tellus A Dyn Meteorol Oceanogr 74:204–221. https://doi.org/10.16993/tellusa.49

Koenigk T et al (2020) On the contribution of internal climate variability to European future climate trends. Tellus A Dyn Meteorol Oceanogr 72(1):1–17. https://doi.org/10.1080/16000870.2020.1788901

Kucerova M et al (2017) Trends in frequency and persistence of atmospheric circulation types over Europe derived from a multitude of classifications. Int J Climatol 37:2502–2521. https://doi.org/10.1002/joc.4861

Kuettel M et al (2011) Multidecadal changes in winter circulation-climate relationship in Europe: frequency variations, within-type modifications, and long-term trends. Clim Dyn 36:957–972. https://doi.org/10.1007/s00382-009-0737-y

Lind P et al (2022) Climate change information over Fenno-Scandinavia produced with a convection-permitting climate model. Clim Dyn. https://doi.org/10.1007/s00382-022-06589-3

Lind P et al (2020) Benefits and added value of convection-permitting climate modelling over Fenno-Scandinavia. Clim Dyn 55:1893–1912. https://doi.org/10.1007/s00382-020-05359-3

Mittermeier M et al (2022) A deep learning based classification of atmospheric circulation types over Europe: projection of future changes in a CMIP6 large ensemble. Environ Res Lett 17:084021. https://doi.org/10.1088/1748-9326/ac8068

Murawski A et al (2018) Do changing weather types explain observed climatic trends in the rhine basin? An analysis of within- and between-type changes. J Geophys Res Atmos 123(3):1562–1584. https://doi.org/10.1002/2017JD026654

Nakicenovic N, Alcamo J, Grubler A, Riahi K, Roehrl RA, Rogner H-H, Victor N (2000) Special report on emissions scenarios (SRES), a special report of working group III of the intergovernmental panel on climate change. Cambridge University Press, Cambridge. ISBN 0-521-80493-0

O'Gorman PA, Schneider T (2009) The physical basis for increases in precipitation extremes in simulations of 21st-century climate change. PNAS. https://doi.org/10.1073/pnas.0907610106

O'Neill BC et al (2016) The Scenario Model Intercomparison Project (ScenarioMIP) for CMIP6. Geosci Model Dev 9:3461–3482. https://doi.org/10.5194/gmd-9-3461-2016

Pall P, Allen MR, Stone DA (2007) Testing the Clausius-Clapeyron constraint on changes in extreme precipitation under CO_2 warming. Clim Dyn 28:351–363. https://doi.org/10.1007/s00382-006-0180-2

Philipp A et al (2007) Long-term variability of daily North Atlantic-European pressure patterns since 1850 classified by simulated annealing clustering. J Clim 20(16):4065–4095. https://doi.org/10.1175/JCLI4175.1

Philipp A et al (2010) Cost733cat-a database of weather and circulation type classifications. Phys Chem Earth 35(9–12):360–373

Røste J, Landgren J (2022) Impacts of dynamical downscaling on circulation type statistics in the Euro-CORDEX ensemble. Clim Dyn. https://doi.org/10.1007/s00382-022-06219-y

Schlesinger ME, Ramankutty N (1994) An oscillation in the global climate system of period 65–70 years. Nature 367(6465):723–726. https://doi.org/10.1038/367723a0

Schneider T et al (2015) Physics of changes in synoptic midlatitude temperature variability. J Clim 28(6):2312–2331. https://doi.org/10.1175/JCLI-D-14-00632.1

Screen JA (2014) Arctic amplification decreases temperature variance in northern mid- to high-latitudes. Nat Clim Change 4:577–582. https://doi.org/10.1038/nclimate2268

ScreenMantua JA et al (1997) A Pacific interdecadal climate oscillation with impacts on salmon production. Bull Am Meteorol Soc 78(6):1069–1079. https://doi.org/10.1175/1520-0477(1997)078%3c1069:APICOW%3e2.0.CO;2

Stryhal J, Huth R (2019a) Classifications of winter atmospheric circulation patterns: validation of CMIP5 GCMs over Europe and the North Atlantic. Clim Dyn 52(5–6):3575–3598. https://doi.org/10.1007/s00382-018-4344-7

Stryhal J, Huth R (2019b) Trends in winter circulation over the British Isles and central Europe in twenty-first century projections by 25 CMIP5 GCMs. Clim Dyn 52(1–2):1063–1075. https://doi.org/10.1007/s00382-018-4178-3

Trenberth KE et al (1997) The definition of El Niño. Bull Amer Meteorol Soc 78:2771–2777

van Vuuren DP, Edmonds J, Kainuma M et al (2011) The representative concentration pathways: an overview. Clim Change 109:5. https://doi.org/10.1007/s10584-011-0148-z

Waugh DW et al (2017) What is the polar vortex and how does it influence weather? Bull Am Meteorol Soc 98(1):37–44

Wilcke RAI et al (2020) The extreme warm summer 2018 in Sweden—set in a historical context. Earth Syst Dyn 11:1107–1121. https://doi.org/10.5194/esd-11-1107-2020

Wilks DS (2011) Statistical methods in the atmospheric sciences, 3rd edn. Academic Press, Oxford

Wyser K et al (2021) The SMHI large ensemble (SMHI-LENS) with EC-Earth3.3.1. Geosci Model Dev 14:4781–4796. https://doi.org/10.5194/gmd-14-4781-2021